Article

Molecular Conductance Switch-On of Single Ruthenium Complex Molecules

Kyoungja Seo, Alexander V. Konchenko, Junghyun Lee, Gyeong Sook Bang, and Hyoyoung Lee

J. Am. Chem. Soc., **2008**, 130 (8), 2553-2559 • DOI: 10.1021/ja077089u

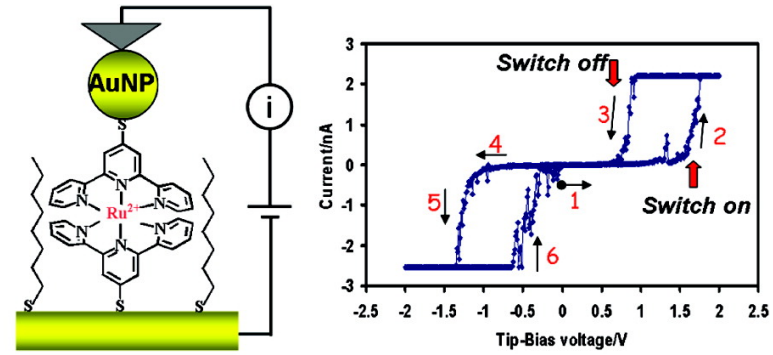

A voltage-driven molecular switch

More About This Article

Additional resources and features associated with this article are available within the HTML version:

- Supporting Information
- Links to the 3 articles that cite this article, as of the time of this article download
- Access to high resolution figures
- Links to articles and content related to this article
- Copyright permission to reproduce figures and/or text from this article

View the Full Text HTML

J|A|C|S
ARTICLES
Published on Web 02/06/2008

Molecular Conductance Switch-On of Single Ruthenium Complex Molecules

Kyoungja Seo, Alexander V. Konchenko, Junghyun Lee, Gyeong Sook Bang, and Hyoyoung Lee*

National Creative Research Initiative, Center for Smart Molecular Memory, Electronics and Telecommunications Research Institute (ETRI), 161 Gajeong-dong, Yuseong-gu, Daejeon 305-350, Korea

Received September 13, 2007; E-mail: hyoyoung@etri.re.kr

Abstract: Thiol-tethered Ru^{II} terpyridine complexes were synthesized for a voltage-driven molecular switch and used to understand the switch-on mechanism of the molecular switches of single metal complexes in the solid-state molecular junction in a vacuum. Molecularly resolved scanning tunneling microscopy (STM) images revealed well-defined single Ru^{II} complexes isolated in the highly ordered dielectric monolayer. When a negative sample-bias was applied, the threshold voltage to the high conductance state in the molecular junctions of the Ru^{II} complex was consistent with the electronic energy gap between the Fermi level of the gold substrate and the lowest ligand-centered redox state of the metal complex molecule. As an active redox center leading to conductance switching in the molecule, the lowest ligand-centered redox state of Ru^{II} complexes was suggested to trap an electron injected from the gold substrate. Our suggestions for a single-molecule switch-on mechanism in the solid state can provide guidance in a design that improves the charge-trapping efficiency of the ligands with different metal substrates.

Introduction

Molecular Switch. Molecular electronic elements are very attractive for applications of nanodevices as alternatives to the high-cost and low-integrated silicon devices.[1−3] As elements in functional molecular electronic devices,[4,5] molecular switches have been designed for the achievement of the concept of a molecular electronic change driven by a photon[6,7] or an electron.[8,9] Redox-active π-conjugated molecules and transition metal complexes having at least two redox states (reduction and oxidation) are promising candidates for application to molecular switches.[10−13] If an applied potential can control the redox states of the molecules sandwiched between two metal contacts, the conducting channel induced by a redox fluctuation can open to the Fermi levels of the contacts and charge transport can occur at a redox state close to the Fermi levels.[14,15] Thus, molecular electronic events such as negative differential resonance (NDR) and conducting switching reflect the electrochemical reaction of molecules.[10,11] Discrete redox states of the molecules via oxidation and reduction reactions can be accessible to transfer and store charges.

Molecular Conductance Switch-On Process. For the design of real applicable molecular devices, current−voltage properties through molecular nanostructures such as metal−molecule−metal junctions (molecular junctions) have been studied extensively.[16−23] Charge transport through the molecular junctions depends significantly on the energy levels of molecules relative to the Fermi levels of the contacts[24,25] and the electronic

(1) Bumm, L. A.; Arnold, J. J.; Cygan, M. T.; Dunbar, T. D.; Burgin, T. P.; Jones, L., II; Allara, D. L.; Tour, J. M.; Weiss, P. S. *Science* **1996**, *271*, 1705.
(2) Collier, C. P.; Wong, E. W.; Belohradsk yacute, M.; Raymo, F. M.; Stoddart, J. F.; Kuekes, P. J.; Williams, R. S.; Heath, J. R. *Science* **1999**, *285*, 391.
(3) Collier, C. P.; Mattersteig, G.; Wong, E. W.; Luo, Y.; Beverly, K.; Sampaio, J.; Raymo, F. M.; Stoddart, J. F.; Heath, J. R. *Science* **2000**, *289*, 1172.
(4) Tour, J. M.; Kozaki, M.; Seminario, J. M. *J. Am. Chem. Soc.* **1998**, *120*, 8486.
(5) Blum, A. S.; Kushmerick, J. G.; Long, D. P.; Patterson, C. H.; Yang, J. C.; Henderson, J. C.; Yao, Y.; Tour, J. M.; Shashidhar, R.; Ratna, B. R. *Nat. Mater.* **2005**, *4*, 167.
(6) Sortino, S.; Petralia, S.; Conoci, S.; Di Bella, S. *J. Am. Chem. Soc.* **2003**, *125*, 1122.
(7) Sortino, S.; Petralia, S.; Conoci, S.; Bella, S. D. *J. Mater. Chem.* **2004**, *14*, 811.
(8) Gittins, D. I.; Bethell, D.; Schiffrin, D. J.; Nichols, R. J. *Nature* **2000**, *408*, 67.
(9) He, H. X.; Li, X. L.; Tao, N. J.; Nagahara, L. A.; Amlani, I.; Tsui, R. *Phys. Rev. B* **2003**, *68*, 045302.
(10) Wassel, R. A.; Credo, G. M.; Fuierer, R. R.; Feldheim, D. L.; Gorman, C. B. *J. Am. Chem. Soc.* **2004**, *126*, 295.
(11) He, J.; Fu, Q.; Lindsay, S.; Ciszek, J. W.; Tour, J. M. *J. Am. Chem. Soc.* **2006**, *127*, 11932.
(12) Xiao, X.; Nagahara, L. A.; Rawlett, A. M.; Tao, N. *J. Am. Chem. Soc.* **2005**, *127*, 9235.
(13) Cai, L.; Cabassi, M. A.; Yoon, H.; Cabarcos, O. M.; McGuiness, C. L.; Flatt, A. K.; Allara, D. L.; Tour, J. M.; Mayer, T. S. *Nano Lett.* **2005**, *5*, 2365.
(14) Albrecht, T.; Guckian, A.; Ulstrup, J.; Vos, J. G. *Nano Lett.* **2005**, *5*, 1451.
(15) Wassel, R. A.; Credo, G. M.; Fuierer, R. R.; Feldheim, D. L.; Gorman, C. B. *J. Am. Chem. Soc.* **2004**, *126*, 295.
(16) Bumm, L. A.; Arnold, J. J.; Dunbar, T. D.; Allara, D. L.; Weiss, P. S. *J. Phys. Chem. B* **1999**, *103*, 8122.
(17) Blum, A. S.; Yang, J. C.; Shashidhar, R.; Ratna, B. *Appl. Phys. Lett.* **2003**, *82*, 3322.
(18) Yu, L. H.; Keane, Z. K.; Ciszek, J. W.; Cheng, L.; Stewart, M. P.; Tour, J. M.; Natelson, D. *Phys. Rev. B* **2004**, *93*, 4.
(19) He, J.; Lindsay, S. M. *J. Am. Chem. Soc.* **2005**, *127*, 11932.
(20) Albrecht, T.; Guckian, A.; Kuznetsov, A. M.; Vos, J. G.; Ulstrup, J. *J. Am. Chem. Soc.* **2006**, *128*, 17132.
(21) Morita, T.; Lindsay, S. *J. Am. Chem. Soc.* **2007**, *129*, 7262.
(22) Li, X. L.; Hihath, J.; Chen, F.; Masuda, T.; Zang, L.; Tao, N. J. *J. Am. Chem. Soc.* **2007**, *129*, 11535.
(23) Adam, M. R.; Theresa, J. H.; Larry, A. N.; Raymond, K. T.; Ganesh, K. R.; Stuart, M. L. *Appl. Phys. Lett.* **2002**, *81*, 3043.
(24) Kitagawa, K.; Morita, T.; Kimura, S. *Langmuir* **2005**, *21*, 10624.

structure of the molecule.[25,26] In the concept of a molecular switch is the idea that the charge can be efficiently trapped in the molecule; a resonant state (a redox state) of molecules as a conducting channel, where that is the highest occupied molecular orbital (HOMO) or the lowest unoccupied molecular orbital (LUMO), may trap charges injected from close Fermi levels of the contacts. In dry samples, however, the relationship between the electronic structure of transition metal complex molecules and charge-trapping processes from the contacts to the molecule has been poorly addressed at molecular levels. For example, charge trapping induced by light or electrons in transition metal complexes on semiconductor surfaces such as In_2O_3 nanowires[26,27] and TiO_2 films[28] as charge-sensitive nanostructures have been reported. Photochemically or electrochemically induced metal-centered or ligand-centered chemical reactions should drive charge or electron trapping into the molecular state. However, in many of the investigations of molecular switches or memory nanodevices including these semiconductor nanostructures, switch-on threshold voltages have not been characterized by $I-V$ characteristics at molecular levels.

Ru^{II} Terpyridine Complex, a Molecular Switch. To understand the voltage-driven switch-on mechanism in the solid-state molecular junction of single-metal complexes, thiol-tethered ruthenium(II) terpyridine complexes were synthesized for a voltage-driven molecular switch. The transition metal MLCT (metal-to-ligand charge transfer) complexes can offer two redox-centered states (i.e., the metal-centered HOMO and the ligand-centered LUMO).[29,30] The chemistry of the metal-centered and ligand-centered reactions for a transition metal−electroactive ligand complex is well understood.[29,30] Ru^{II}-centered complexes exhibit stability in their chemical and electronic properties during redox reactions. For measurement of charge transport characteristics of the Ru^{II} complex, the molecular structures were designed to have a centered Ru and mono- or dithiol-substituted terpyridine ligand groups in the molecular junctions between two metal contacts. In addition, Au nanoparticle attachment on the dithiol-tethered Ru^{II} terpyridine complexes incorporated in *n*-alkanethiol self-assembled monolayers (SAMs) was used a simplified symmetric molecular junction, Au-NP/Ru^{II} terpyridine/Au substrate, as a model close to the realistic systems of a molecular switch.

The thiol-tethered Ru^{II} terpyridine complexes in SAMs were characterized using UV−visible absorption spectroscopy, cyclic voltammetry, and scanning tunneling microscopy (STM). To achieve single-molecular junctions, thiol-tethered Ru^{II} terpyridine complexes incorporated in *n*-alkanethiol matrixes (e.g., 1-octanethiol (OT) or 1-dodecanethiol (DDT) SAMs) on Au(111) were prepared, as depicted in Figure 1. The bias-induced conductance switching of Ru^{II} complexes in the single-molecular junctions was probed by using scanning tunneling spectroscopy (STS) in an ultrahigh vacuum. A proposed mechanism for voltage-driven switch-on is that the electron can be trapped from metal contacts to the ligand-centered LUMO. Our results will provide sufficient motivation to design various ligands and to investigate "charge trapping" with different work functions of metal contacts in the solid state.

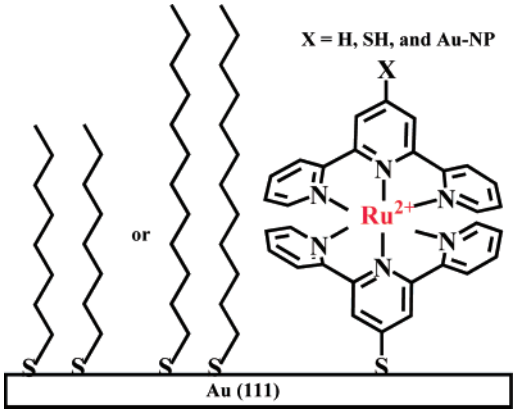

Figure 1. Scheme of Ru^{II} complexes incorporated in an ordered *n*-alkanethiol SAM on Au(111).

Experimental Section

Mono- and diacetylthiol-tethered Ru^{II} terpyridine complexes ((2,2′:6,2″-terpyridinyl)(4′-acetylthioalkyl-2,2′:6,2″-terpyridinyl))ruthenium(II) hexafluorophosphate, $[Ru^{II}(tpy)(tpy(CH_2)_nSAc)](PF_6)_2$, $n = 0$, 7, 13, and bis(4′-acetylthiol-2,2′:6,2″-terpyridinyl)ruthenium(II) hexafluorophosphate, $[Ru^{II}(tpySAc)_2](PF_6)_2$, denoted by $Ru^{II}(tpy)(tpyC_nSAc)$ and $Ru^{II}(tpySAc)_2$, respectively, in this paper) were synthesized as described in a previous report.[31] Deprotection of the thioacetate group to generate active sulfur adsorbing on Au(111) was conducted by mixing ~15 μL of ammonium hydroxide (NH_4OH, Aldrich) with a 5 mL acetonitrile solution of 1 mM $Ru^{II}(tpy)(tpyC_nSAc)$. This solution was diluted with acetonitrile again before use for the formation of each monolayer.

All samples for the STM experiments were prepared on an Au(111) on mica substrate (Molecular Imaging). The substrate was cleaned with a hot piranha solution (1:3 H_2O_2 (Junsei) and H_2SO_4 (Junsei)) (*Caution! Piranha solution is a very strong oxidant and is extremely dangerous to work with; gloves, goggles, and a face shield should be worn*), washed with DI water and ethanol, dried with N_2 gas, and annealed with a propane flame before use.

SAMs of Ru^{II} terpyridine complexes on Au(111) were prepared as follows: (1) A single component $Ru^{II}(tpy)(tpyC_nS)$ SAM was formed in a 0.1 mM solution at 60 ± 5 °C for 2 hours. (2) Incorporation of a single molecule or molecular bundles of $Ru^{II}(tpy)(tpyC_nS)$ into a *n*-alkanethiol matrix on Au(111) was conducted by immersion of the *n*-alkanethiol SAMs, formed in a 1 mM ethanol solution at room temperature for 2 hours, in a 10−50 μM acetonitrile solution of $Ru^{II}(tpy)(tpyC_nS)$ or $Ru^{II}(tpyS)_2$ at 60 ± 5 °C for 2 hours. (3) For the attachment of gold nanoparticles, the $Ru^{II}(tpyS)_2$ incorporating the OT SAM was immersed in a solution containing 5 nm gold nanoparticles, Au-NPs (stored in a refrigerator, Aldrich) overnight. (4) All SAMs on Au(111) for STM experiments were washed with solvents such as ethanol and acetone to remove physisorbed molecules from the surfaces, dried with N_2 gas, and immediately transferred to a STM vacuum chamber.

STM (Omicron, UHV VTSTM) was performed at room temperature in an ultrahigh vacuum ($< 1.5 \times 10^{-10}$ Torr). Electrochemically etched Pt/Ir tips (Molecular Imaging) were used for STM and STS. All STM images were recorded in the constant current mode. For reliable $I-V$ measurements in single-molecule junctions, it was initially attempted

(25) Kim, B. S.; Beebe, J. M.; Olivier, C.; Rigaut, S.; Touchard, D.; Kushmerick, J. G.; Zhu, X. Y.; Frisbie, C. D. *J. Phys. Chem. C* **2007**, *111*, 7521.
(26) Li, C.; Fan, W.; Straus, D. A.; Lei, B.; Asano, S.; Zhang, D.; Han, J.; Meyyappan, M.; Zhou, C. *J. Am. Chem. Soc.* **2004**, *126*, 7750.
(27) Li, C.; Ly, J.; Lei, B.; Fan, W.; Zhang, D.; Han, J.; Meyyappan, M.; Thompson, M.; Zhou, C. *J. Phys. Chem. B* **2004**, *108*, 9646.
(28) Hoertz, P. G.; Thompson, D. W.; Friedman, L. A.; Meyer, G. J. *J. Am. Chem. Soc.* **2002**, *124*, 9690.
(29) Balzani, V.; Juris, A.; Venturi, M.; Campagna, S.; Serroni, S. *Chem. Rev.* **1996**, *96*, 759.
(30) Sauvage, J. P.; Collin, J. P.; Chambron, J. C.; Guillerez, S.; Coudret, C.; Balzani, V.; Barigelletti, F.; De Cola, L.; Flamigni, L. *Chem. Rev.* **1994**, *94*, 993.
(31) Lee, J. H.; Seo, K.; Bang, G. S.; Choi, N. J.; Lee, H. Submitted for publication.

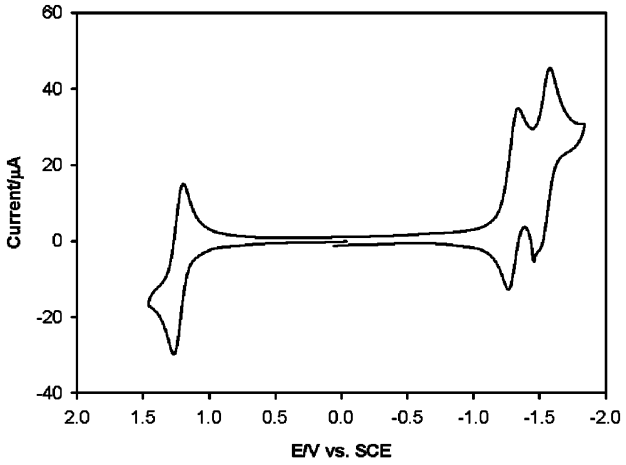

Figure 2. Cyclic voltammogram for a 3 mM $Ru^{II}(tpy)(tpyC_{13}SAc)$ solution in acetonitrile containing 0.1 M $(TBA)PF_6$ at 0.1 V s^{-1} using a glassy carbon electrode.

to observe a single molecule, and reproducible $I-V$ curves from the single molecule were obtained in the current dynamic range of ±2.5 nA.

Cyclic voltammetry was performed at room temperature (CHI, Electrochemical Analyzer 660A) under an N_2 atmosphere. All solutions for voltammetric experiments were degassed with N_2 gas. UV−vis absorption spectroscopy was performed at room temperature (Hitachi, U-3501 UV/vis/NIR spectrophotometer). All SAMs for cyclic voltammetry and UV−vis absorption spectroscopy were prepared in 3 mM solutions of $Ru^{II}(tpy)(tpyC_nSAc)$, $n = 7$ and 13, at room temperature for 24 hours, washed with acetonitrile and acetone, and dried with N_2 gas.

Results and Discussion

Electrochemical and Photochemical Characterization of Ru^{II} Terpyridine Complexes. Discrete redox states due to metal- and ligand-centered reactions of Ru^{II} terpyridine complexes were clearly characterized by cyclic voltammetry (Figure 2). The redox formal potential respective to the Ru^{III}/Ru^{II} reaction was approximately +1.2 V_{SCE}. The first two redox couples of terpyridine ligand were observed in the negative potential region, and the first redox formal potential respective to the $[Ru^{II}(tpy)_2]^{2+}/[Ru^{II}(tpy)(tpy)^-]^+$ reaction was approximately −1.2 V_{SCE}. On the other hand, the typical MLCT electronic transition (λ_{max} = 477 nm) of Ru^{II} terpyridine complexes was characterized by the UV−vis absorption spectra (Figure S1A, Supporting Information). The Ru^{II} terpyridine complex SAMs on an indium-tin oxide (ITO) electrode were also characterized photochemically by the MLCT electronic transition in the UV−vis adsorption spectra of the solid state (Figure S1B, Supporting Information) and electrochemically by well-defined redox current peaks of Ru^{III}/Ru^{II} with a surface coverage of 7.4×10^{-11} mol cm^{-2} (Figure S1C, Supporting Information). Surface coverage for the corresponding electroactive Ru^{II} moieties was calculated from the charge under the oxidation and reduction peaks of cyclic voltammograms (CVs). The peak currents of the monolayer show a linear increase with the scan rate, as expected for the redox-active system bound on the surface (Figure S1D, Supporting Information).[32]

Scanning Tunneling Microscopy and Spectroscopy under Vacuum Conditions. STM images for the $Ru^{II}(tpy)(tpyS)$ SAMs on Au(111) showed molecular globes presumed to be individual molecules or molecular bundles while an ordered structure of Ru^{II} terpyridine complex SAMs was not observed (Figure 3A). To construct single molecular junctions in dielectric barriers, the incorporation of Ru^{II} terpyridine complexes was conducted in *n*-alkanethiol SAMs, and single molecules or molecular bundles of $Ru^{II}(tpy)(tpyS)$ were observed as protrusions at the edge of gold vacancy islands and at the domain boundaries of well-ordered *n*-alkanethiol (Figure 3B). The number of incorporated Ru^{II} terpyridine complexes was controlled by the concentration (1 μM−0.1 mM) and immersion time periods (20 minutes−2 hours). We demonstrated bias-induced switching originating from the intrinsic nature of Ru^{II} terpyridine complexes using different molecular junctions of $Ru^{II}(tpy)(tpyC_nS)$, $Ru^{II}(tpyS)_2$, and Au-NP-capped $Ru^{II}(tpyS)_2$ constructed in DDT and OT SAMs. If a dielectric barrier was short (e.g., a $Ru^{II}(tpy)(tpyS)$-incorporated OT SAM), the number of incorporated $Ru^{II}(tpy)(tpyS)$ molecules as bright protrusions increased at the edge of the gold vacancy islands and at the boundaries of the ordered OT domains (Figure 3B) compared to a $Ru^{II}(tpy)(tpyS)$-incorporated DDT SAM (Figure 4A). Most of the bright protrusions were continuously imaged, while some of them rarely displayed stochastic switching as the molecules blinked on and off in the STM images.[33,34] Single molecules or molecular bundles of the Ru^{II} terpyridine complex were defined by a cross-sectional analysis of STM images. The size of the Ru^{II} terpyridine complex (i.e., $Ru^{II}(tpy)_2$) was estimated to be 11.3 Å according to MM2 calculations in ChemBats3D. STM images reflect the conductance and physical height/length, which allows the physical difference to be determined if imaged Ru^{II} terpyridine complexes are single molecules or molecular bundles. From the results of a cross-sectional analysis of both STM images for a pure $Ru^{II}(tpy)(tpyS)$ SAM and a $Ru^{II}(tpy)$-(tpyS)-incorporated OT SAM, molecular globes or white

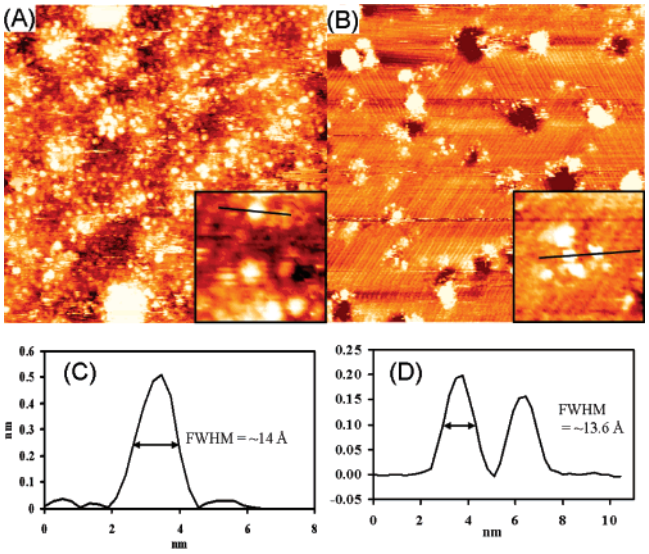

Figure 3. STM images (88 × 88 nm^2) of (A) a pure $Ru^{II}(tpy)(tpyS)$ SAM and (B) a $Ru^{II}(tpy)(tpyS)$-incorporated 1-octanethiol (OT) SAM on Au(111) at a constant tunneling current of 20 pA with a tip-bias of 1.2 V in a vacuum. (C, D) Cross-sectional analysis for the inset images A and B, respectively.

(32) Bard, A. J.; Faulkner, L. R. *Electrochemical Methods, Fundamentals and Applications*; John Wiley & Sons: New York, 1980.

(33) Donhauser, Z. J.; Mantooth, B. A.; Kelly, K. F.; Bumm, L. A.; Monnell, J. D.; Stapleton, J. J.; Price, D. W., Jr.; Rawlett, A. M.; Allara, D. L.; Tour, J. M.; Weiss, P. S. *Science* **2001**, *292*, 2303.

(34) Basch, H.; Cohen, R.; Ratner, M. A. *Nano Lett.* **2005**, *5*, 1668.

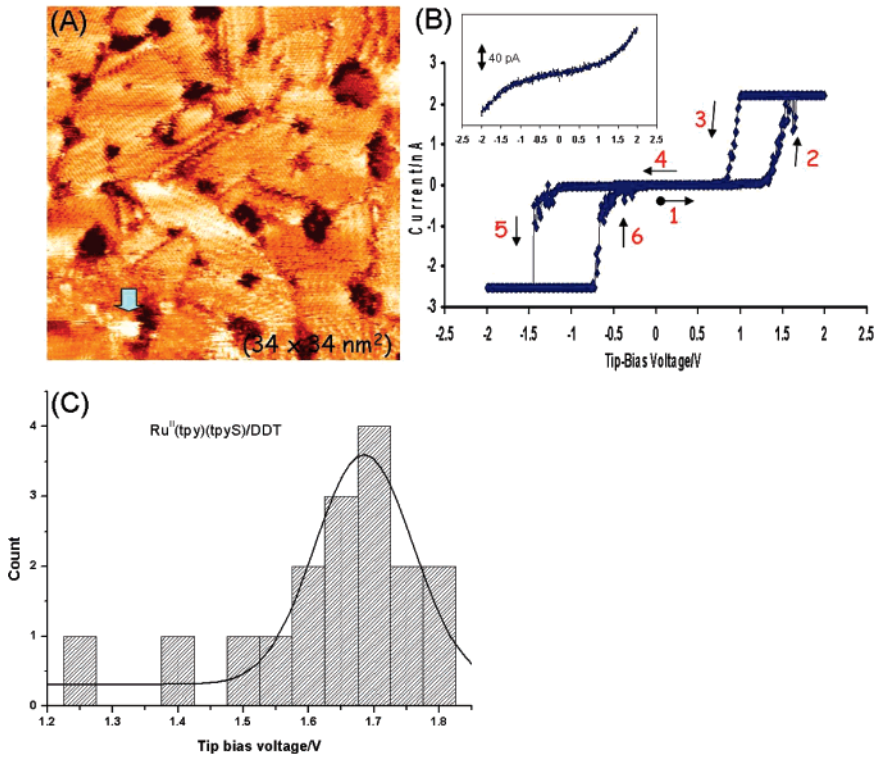

Figure 4. (A) STM image (34 × 34 nm^2) of a Ru^{II}(tpy)(tpyS)-incorporated 1-dodecanethiol (DDT) SAM on Au(111). The image was obtained at a constant tunneling current of 20 pA with a tip-bias of 1.2 V in a vacuum. (B) Current−voltage (*I*−*V*) characteristics measured from a Ru^{II}(tpy)(tpyS) molecule marked with an arrow in (A). The inset is an *I*−*V* curve measured from the DDT molecule. (C) Histograms of the threshold voltage for the current switch-on in the single Ru^{II}(tpy)(tpyS) junctions. The solid line is a Gaussian fit. *I*−*V* curves were measured from single Ru^{II}(tpy)(tpyS) molecules without a tunneling current feedback.

protrusions that are approximately 13−14 Å in the fwhm (full width at half-maximum) could be defined as a single molecule (Figure 3C,D) in which larger molecular globes such as those that are >20 Å could be defined as molecular bundles (Figure S2, Supporting Information). On the other hand, a cross-sectional analysis of a STM image for a Ru^{II}(tpy)(tpyS)-incorporated DDT SAM (Figure S3, Supporting Information) showed that the fwhm for a white protrusion is approximately 22 Å, which is likely a bundle of Ru^{II} terpyridine complexes.

After successive STM imaging for the Ru^{II}(tpy)(tpyS)-incorporated DDT SAM (Figure 4A), the current−voltage (*I*−*V*) curves of the current response to the tip-bias voltage were measured from the Ru^{II}(tpy)(tpyS) molecule marked with an arrow (in Figure 4A) without tunneling current feedback. The current values were recorded while the tip-bias voltage was swept from zero to positive or negative directions in a cycle. After the current−voltage measurement was finished, the current feedback was restored and tip-scanning continued. This procedure was performed for all molecular junctions. A representative *I*−*V* curve for a molecular junction of Ru^{II}(tpy)(tpyS) is shown in Figure 4B. The tip-bias voltage was swept in a cycle, 0 V → +2 V → 0 V → −2 V → 0 V. Hysteretic *I*−*V* curves were obtained in both sweep directions. *I*−*V* curves were measured 2 or 3 times on the top of the same protrusions repeatedly during one scan. The average number of reproducible cycles for hysteretic *I*−*V* curves was two, which strongly depended on the drift condition of the STM system. Thus, for a statistical analysis, hysteretic *I*−*V* curves obtained from the results of several scans for different protrusions were used. When a positive tip-bias was applied, 0 V → +2 V → 0 V (i.e., application of a negative bias to the sample), the tunneling currents suddenly increased after approximately 1.5 V and then returned to a residual current flow at approximately 0.7 V with the reverse scan (Figure 4B). However, conductance switching for the single DDT molecules used for a control experiment was not observed as shown in the inset of Figure 4B, and the curves showed symmetrical and sigmoidal *I*−*V* characteristics. The histograms of the threshold voltage for the current switch-on in molecular junctions of the Ru^{II}(tpy)(tpyS)-incorporated DDT SAM suggest that the molecule switched to a high conductance state primarily at 1.70 ± 0.025 V (Figure 4C). On the other hand, in molecular junctions of the Ru^{II}(tpy)(tpyS)-incorporated OT SAM, the molecule switched primarily to a high conductance state at approximately 1.75 ± 0.025 V, as shown in the histograms of the threshold voltage for the current switch-on (Figure S4, Supporting Information). This type of conductance switching was observed in all molecular junctions with Ru^{II} terpyridine molecules, including Ru^{II}(tpy)(tpyC$_n$S), *n* = 7 and 13 (not shown).

The molecular junctions with a dithiol-tethered Ru^{II} terpyridine complex (i.e., Ru^{II}(tpyS)$_2$) formed in an OT SAM. Figure 5 shows STM images of dithiol-tethered Ru^{II} terpyridine complexes incorporated into the OT SAM (Figure 5A) and a statistical analysis of the threshold voltage for the current switch-on (Figure 5B). The molecular junctions consisted of the STM tip/one free thiol group of the Ru^{II}(tpyS)$_2$/Au substrate. Single or bundles of Ru^{II}(tpyS)$_2$ molecules as well as monothiol-tethered Ru^{II} terpyridine complexes (i.e., Ru^{II}(tpy)(tpyS)) were observed as bright protrusions in the OT SAM. Some of the protrusions at the edge of the gold vacancy islands occasionally displayed stochastic switching. However, the protrusions at the boundaries of the ordered OT domains were imaged stably and

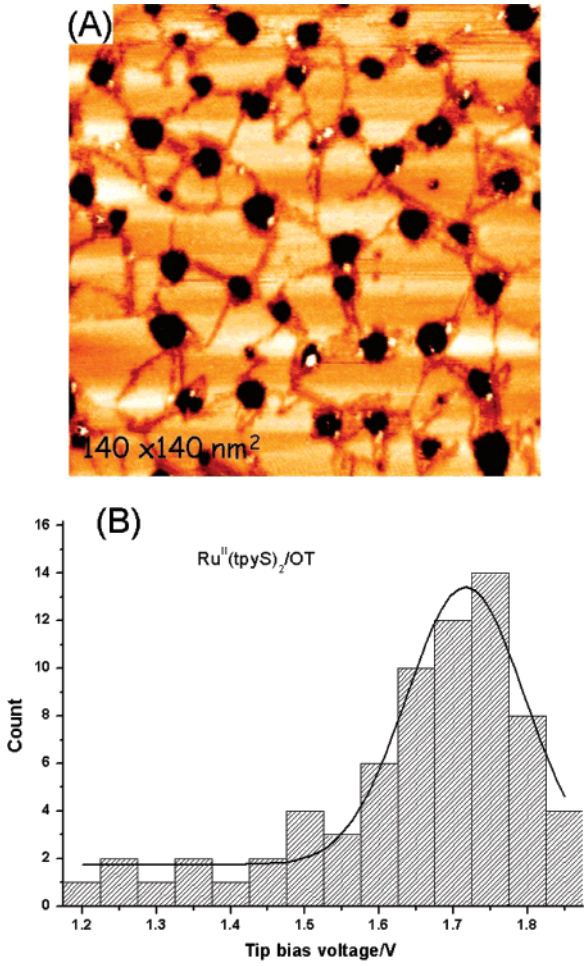

Figure 5. (A) STM image of a $Ru^{II}(tpyS)_2$-incorporated 1-octanthiol (OT) SAM on Au(111) at a constant tunneling current of 20 pA with a tip-bias of 1.2 V. (B) Histograms of the threshold voltage for the current switch-on in the single $Ru^{II}(tpyS)_2$ junctions. The solid line is a Gaussian fit. $I-V$ curves were measured from single $Ru^{II}(tpyS)_2$ molecules without a tunneling current feedback.

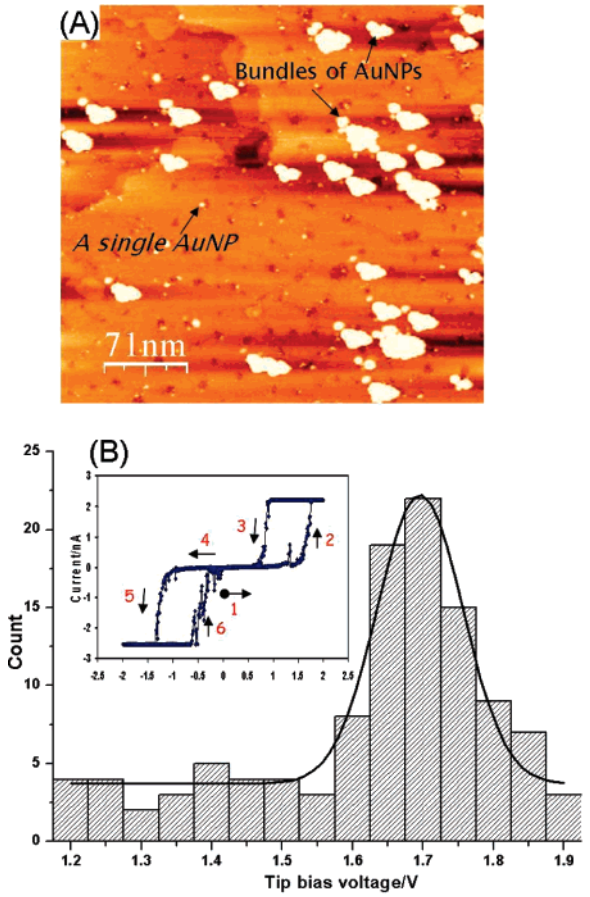

Figure 6. (A) STM image of a Au-NPs-capped $Ru^{II}(tpyS)_2$-incorporated 1-octanethiol (OT) SAM on Au(111). The image was obtained at the constant tunneling current of 20 pA with a tip-bias of 1.2 V in a vacuum. (B) Histograms of the threshold voltage for the current switch-on in the single Au-NP/$Ru^{II}(tpyS)_2$ junctions. The solid line is a Gaussian fit. The inset is an $I-V$ curve measured from an ~5 nm bright spot presumed as Au-NP/$Ru^{II}(tpyS)_2$ without tunneling current feedback.

the hysteretic $I-V$ characteristics were measured from the protrusions reproducibly in both sweep directions (not shown). In the junction of the tip/$Ru^{II}(tpyS)_2$/substrate, the threshold voltage for the current switch-on takes place primarily at 1.75 ± 0.025 V (Figure 5B) in a positive tip-bias direction of 0 V → +2 V → 0 V.

On the other hand, as a model close to realistic systems of a molecular switch, the simplified symmetric molecular junctions of the Au-NP/$Ru^{II}(tpyS)_2$/Au substrate were formed via the attachment of 5 nm gold nanoparticles (Au-NPs) on the top of the inserted dithiol-tethered $Ru^{II}(tpyS)_2$ in the OT SAM (Figure 6A). Single and bundles of Au-NPs were observed at the edge of the gold vacancy islands and at the boundaries of ordered OT domains. $I-V$ curves of single Au-NP junctions showed stable current hysteresis in both bias directions (the inset of Figure 6B), compared to the $I-V$ curves of bundled Au-NP junctions that sometimes show hysteretic $I-V$ characteristics in only one bias direction. However, current hysteresis in only one bias direction was occasionally observed in molecular junctions of Ru^{II} terpyridine complexes. This may be due to unstable molecular junctions. In this work, this phenomenon was disregarded. On the other hand, in Au-NP junctions, $I-V$ curves can show a charging effect of the nanoparticle,[21,35] which is dependent on the nanoparticle size. According to a previous report,[21] smaller nanoparticles (1.5 nm) had a greater charging effect compared to larger nanoparticles (5.4 nm). The apparent conductance is theoretically smaller by 10% than the actual molecular conductance in the case of a 5.4 nm nanoparticle, which can appear as a wide current-suppressed region in $I-V$ curves.[21] However, magnified $I-V$ curves for the Au-NP/Ru^{II}-$(tpyS)_2$ junctions at an approximate zero bias condition were nearly linear without noticeable current-suppressed regions (not shown); slight oscillation was also observed, which can be attributed to the thermal fluctuation.

The molecular conductance switch-on of the Au-NP-capped molecular junctions takes place primarily at 1.70 ± 0.025 V (according to the histograms in Figure 6B) in a positive tip-bias direction of 0 V → +2 V → 0 V. Therefore, the results of conducting switching in different junctions with mono- and dithiol-tethered Ru^{II} terpyridine complexes demonstrate that the bias-induced switching occurs due to the intrinsic nature of the molecules, although the role of the internal conformation change cannot be ignored. The switch-on threshold voltage of Ru^{II} terpyridine complexes in the molecular junctions, gold (or Pt/

(35) Hanna, A. E.; Tinkham, M. *Phys. Rev. B* **1991**, *44*.

Ir)/Ru^{II} terpyridine complexes/gold substrate, can be approximated in the range 1.70−1.75 V.

Proposed Model for Electron Trapping in Ru^{II} Terpyridine Complexes. When the Fermi levels of electrodes align to molecular redox formal potentials, resonant tunneling may take place across reduction−oxidation states which can be expected due to the chemical nature of the charge-trap states. Vacuum levels of the ionization and the electron affinity of molecules on metals can be closely approximated from electrochemical potential scales. The first electrochemical oxidation and reduction potentials should be approximately the first ionization energy and the first electron affinity levels of thin film supported on metals, respectively.[36] To convert an electrochemical potential referenced to a saturated calomel electrode (SCE) to a vacuum level, it is possible to utilize the simplified model offered by Hipps et al.,[11,36,37] $V_{abs}(eV) = 4.7\ eV + E^0(SCE)$, in which E^0 is the redox formal potential and 4.7 eV is approximated according to the vacuum level, ∼4.5 eV for the NHE (normal hydrogen electrode) and a 0.24 V difference between the SCE and the NHE reference electrode.[38] For reduction processes, this model was in very good agreement with UPS (ultraviolet photoelectron spectroscopy) observations in many cases.[36] However, the polarization stabilization of ions by the surrounding molecules and image charges induced in the metal substrate can lead to the ionization potential of electrochemical reactions greater than that of the gas phase (e.g., it was to be approximately 0.5−1.0 eV for a thin film of NiOEP)[36] Thus, for oxidation processes (e.g., the metal-centered oxidation of a transition metal−organic ligand complex), the equation offered by Armstrong et al.[37,39] was used, and the ionization energies $V_i = 4.7\ eV + (1.7)E^{ox}(SCE)_{1/2}$, in which $E^{ox}(SCE)_{1/2}$ is the half-wave oxidation potential. Therefore, the redox formal potentials can be converted to comparable solid-state potentials in STM using two equations, $V_a = 4.7\ eV + E^{red}(SCE)_{1/2}$ and $V_i = 4.7\ eV + (1.7)E^{ox}(SCE)_{1/2}$, where $E^{red}(SCE)_{1/2}$ and $E^{ox}(SCE)_{1/2}$ are the half-wave reduction and oxidation potentials, respectively.

A simplified molecular orbital diagram for an octahedral transition metal complex,[29] which consists of two discrete redox states (the metal-centered highest occupied molecular orbital (HOMO) and the ligand-centered lowest unoccupied molecular orbital (LUMO)), can be used in molecular orbital configurations of Ru^{II}(tpy)(tpyS) as depicted in Figure 7. From the results of electrochemical measurements (Figure 2), the first oxidation occurs near +1.2 V_{SCE} (i.e., $Ru^{II} - e^- \rightarrow Ru^{III}$) and the first reduction occurs near −1.2 V_{SCE} (i.e., $[Ru^{II}(tpy)_2]^{2+} + e^- \rightarrow [Ru^{II}(tpy)(tpy)^-]^+$). These redox formal potentials can be converted to the vacuum levels using two equations offered by Hipps et al.[36] and Armstrong et al.,[39] and the energy levels of the first metal-centered oxidation and the first ligand-centered reduction are 6.74 and 3.4 V below the vacuum, respectively ($V_i = 4.7\ eV + (1.7) \times 1.2 = 6.74\ eV$ and $V_a = 4.7\ eV - 1.2 = 3.4\ eV$). Actual solid-state ionization and electron affinity energies of HOMO and LUMO in the monolayer should deviate slightly from those in a vacuum.[36] However, charge transport can be discussed in terms of the relative energy levels between the LUMO and HOMO levels and metal Fermi levels.[10,24] When a negative or positive bias is applied to the sample, the metal Fermi level of either Pt/Ir or gold should go up toward a molecular orbital level of the Ru^{II} terpyridine complex to allow electron trapping from the metal nearby. The Fermi levels of the STM tip (Pt/Ir) and the substrate (gold) are approximately 5.6 and 5.1 V below the vacuum, respectively.[24] Electron-transfer reactions should occur through the LUMO level because a HOMO level is far from the metal Fermi levels. Application of a negative sample bias drives the Fermi levels of the gold substrate to align to the ligand-centered LUMO of the Ru^{II} terpyridine complexes (Figure 7). Thus, approximately 1.7 V (5.1 V − 3.4 V = 1.7 V) of bias is needed to bring the Fermi level of the gold substrate up to the ligand-centered formal potential, which is close to the typically observed threshold voltage of 1.70−1.75 V.

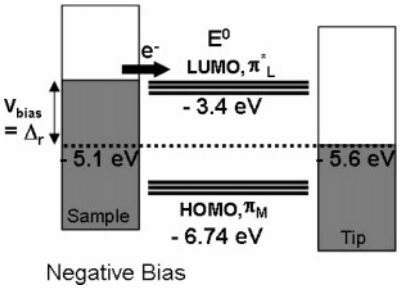

Figure 7. Proposed charging process into the ligand-centered LUMO of Ru^{II} terpyridine complexes. π^*_L and π_M are the molecular orbitals for ligand-centered and metal-centered redox reactions, respectively. E^0 is the redox potential of the molecule. Δ_r denotes the energy of the lowest ligand-centered LUMO state on the substrate.

For an understanding of the hysteretic $I-V$ characteristics in a negative tip-bias direction of 0 V → −2 V → 0 V, the threshold voltage of the current switch-on was analyzed in both molecular junctions in the Ru^{II}(tpy)(tpyS)/gold substrate and the Au-NP/$Ru^{II}(tpyS)_2$/gold substrate. When a negative bias is applied to the tip (0 V → −2 V → 0 V), Pt/Ir should go up toward a molecular orbital level of the Ru^{II} terpyridine complex and the threshold voltage of the conductance switch-on should be larger than that obtained in a positive bias direction due to the different metal Fermi levels between gold and Pt/Ir (see an energy diagram in Figure 7). In molecular junctions of the Pt/Ir tip/Ru^{II}(tpy)(tpyS)/gold substrate, the threshold voltage of −1.95 ± 0.025 V was primarily measured for the current switch-on (Figure S5A, Supporting Information), which roughly agreed with the expected effect. However, the distribution of the threshold voltage is fairly broad. On the other hand, in simplified symmetric Au-NP/$Ru^{II}(tpyS)_2$ junctions (i.e., Pt/Ir tip/Au-NP/$Ru^{II}(tpyS)_2$/gold substrate), Au nanoparticle capping had a significant effect on the threshold voltage values. Histograms of the threshold voltage revealed that the current switch-on takes place primarily at −1.75 ± 0.025 V (Figure S5B, Supporting Information), the absolute value of the threshold voltage that is consistent with that determined in a positive tip-bias direction. In the Au-NP/$Ru^{II}(tpyS)_2$/gold substrate junctions, Ru^{II} terpyridine complexes were supported on gold in both contacts in which the absolute threshold voltage for current switch-on may be similar in both bias directions.

(36) Hipps, K. W. Scanning Tunneling Spectroscopy. In *Handbook of Applied Solid State Spectroscopy*; Vij, D. R., Ed.; Springer-Verlag: Berlin, 2006; Chapter 7.
(37) Scudiero, L.; Barlow, D. E.; Hipps, K. W. *J. Phys. Chem. B* **2002**, *106*, 996.
(38) Memming, R. *Comprehensive Treatise of Electrochemistry*; Conway, B. C., Ed.; Plenum: New York, 1983; Vol 7, Chapter 8.
(39) Schmidt, A.; Armstrong, N. R.; Goeltner, C.; Muellen, K. *J. Phys. Chem.* **1994**, *98*, 11780.

In the all molecular junctions of Ru^{II} terpyridine complexes including simplified symmetric junctions of an Au-NP-capped Ru^{II} dithiol-tethered terpyridine complex, the threshold voltage of switch-on was comparable to the first redox formal potential of the terpyridine ligand supported on gold. The proposed model can postulate that trapping the electron on the ligand center of Ru^{II} terpyridine complexes leads to conductance switching.

Conclusion

In summary, the hysteretic $I-V$ characteristics in single-molecular junctions of mono- and dithiol-tethered Ru^{II} terpyridine complexes are reported in a vacuum. The tunneling current initially stays switched off until the sharp threshold voltage is aligned with the electronic energy of the ligand-centered LUMO, which originates with the reduction of the terpyridine ligand. Thus, the threshold voltage can be determined by the electronic energy gap between the Fermi level of the metal contacts and the lowest ligand-centered redox state of the metal complex molecule. For molecular memory applications, these results can provide guidance in design that improves the charge-trapping efficiency of various ligands with different metal substrates in the solid state. Further study regarding the construction of molecular junctions with different metal contacts and examination of the function of metal contacts on the switch-on of molecules is underway.

Acknowledgment. This work was supported by the Creative Research Initiatives (project title: Smart Molecular Memory) of the MOST/KOSEF.

Supporting Information Available: Photochemical and electrochemical characterization of Ru^{II} terpyridine complexes (Figure S1), STM images and cross-sectional data for the Ru^{II}-(tpy)(tpyS)-incorporated OT and DDT SAMs (Figures S2 and S3), and histograms of the threshold voltage for the current switch-on in the molecular junctions of Ru^{II}(tpy)(tpyS) (Figures S4 and S5A) and Au-NP-capped Ru^{II}($tpyS_2$) (Figure S5B). This material is available free of charge via the Internet at http://pubs.acs.org.

JA077089U